

Computational hybrid imaging

Yi Xue¹, Laura Waller^{1,*}

¹*Department of Electrical Engineering & Computer Sciences, University of California, Berkeley, CA, USA*

**Corresponding author: waller@berkeley.edu*

Abstract

Fluorescence microscopy is a powerful tool to measure molecular specific information in biological samples. However, most biological tissues are highly heterogeneous because of refractive index (RI) differences and thus degrade the signal-to-noise ratio of fluorescence images. At the same time, RI is an intrinsic optical property of label free biological tissues that quantitatively relates to cell morphology, mass, and stiffness. Conventional imaging techniques measure fluorescence and RI of biological samples separately. Here, we develop a new computational hybrid imaging method based on a multi-slice model of multiple scattering that reconstructs 3D fluorescence and 3D RI from the same dataset of fluorescence images. Our method not only bridges the gap between fluorescence and RI imaging and provides a panoramic view of the biological samples, but also can digitally correct multiple scattering effect of fluorescence images from the reconstructed 3D RI. Computational hybrid imaging opens a unique avenue beyond conventional imaging techniques.

Main

Fluorescence microscopy's utility is often hindered by light scattering, which limits imaging depth. Scattering is mainly caused by the heterogeneity of different structures of the tissue, that is, refractive index (RI). Knowing the RI will not only help correct scattering and extend fluorescence imaging depth but also provide quantitative information of the tissue such as protein concentration and dry mass.

Even though measuring RI of tissues and imaging through scattering tissues are closely related, to our knowledge, no existing method could reconstruct both RI and fluorescence signals from the same dataset. Previous works either only focus on reconstruct fluorescence signals by phase conjugate and wavefront shaping¹⁻³, ultrasound-assisted optical imaging⁴⁻⁷, measurement of transmission^{8,9} or reflection matrix^{10,11}, and computational optimization¹²⁻¹⁶; or they focus on measure RI but not fluorescence by optical diffraction tomography¹⁷⁻¹⁹, computational phase retrieval²⁰⁻²⁴, and optical coherence refractive tomography²⁵. Only very rare works record both fluorescence and phase information of the same samples²⁶⁻²⁹, but they require independent experiments and measurements to reconstruct these two types of signals respectively. In addition, most of RI measurements based on tomography are in transmission geometry which limits the application for *in vivo* imaging.

Here, we exploit fluorescence as 'light sources' inside of a sample, illuminating non-labeled tissue as it propagates through. Fluorescence images recorded on top of the sample consists of scrambled fluorescence and RI information. To test this approach, we develop a computational hybrid imaging (CHI) method that exploits a physics-based multi-slice model for multiple scattering to unscramble fluorescence and RI information together from fluorescence images. Our primary goal is to reconstruct RI of non-labeled objects from fluorescence images, since reconstructing 3D fluorescence from 2D fluorescence images is relatively straightforward. We first stimulate a small region of the fluorescence-labeled objects, as a new light source emitting

incoherent spherical wave regardless of the excitation light. In our experiment, we modulate collimated laser light at 473nm wavelength with a Digital Micromirror Device (DMD) as a projector to ‘point-scan’ the sample and collect thousands fluorescence images as the raw data of forward measurements. Note that we take fluorescence images on the top surface of the sample rather than focusing on the fluorescence objects or on the non-labeled objects, in order to collect the intensity of the forward propagated light field carrying 3D fluorescence and 3D RI information. The number of raw measurements depends on the scanning steps.

Next, we select some images from the raw data based on fluorescence intensity distribution as selected forward measurements for reconstruction. Good forward measurements should have high signal-to-noise ratio (SNR) and large light-up areas. The size of the light-up area is proportional to the distance between the fluorescence light source and the image plane. In the multi-slice model, the fluorescence sources inside of the tissue, denoted by $o_f(\mathbf{r})$, is modeled as a spherical wave. The multi-slice model specifically approximates the bulk tissue as a series of thin layers, where the RI of k th layer is denoted by $n_k(\mathbf{r})$. Light propagation through the tissue is modeled via sequential layer-to-layer propagation of the electric field. The intensity of exit electric field at the image plane z , $I_l(\mathbf{r}; z)$, accounting for the accumulation of the diffraction and multiple scattering process are recorded by a camera as the l th forward measurement of our model (Fig. 1). Both 3D fluorescence distribution $o_f(\mathbf{r})$ and 3D RI $n(\mathbf{r})$ are unknown in the model. However, the approximate position of fluorescence objects, especially in the lateral direction, is approximately the center of gravity of the fluorescence image, which is the initial value of $o_f(\mathbf{r})$. Therefore, we first estimate the 3D fluorescence distribution $o_f(\mathbf{r})$ from multiple 2D fluorescence images and then use the expected fluorescence positions to estimate the 3D RI $n(\mathbf{r})$ by solving an optimization problem with Tikhonov regularization R :

$$\operatorname{argmin}_{n(\mathbf{r})} \sum_l \left\| I_l(\mathbf{r}; z) - \hat{I}_l(\mathbf{r}; z) \right\|_2^2 + R[n(\mathbf{r})]. \quad (1)$$

The details about the forward model and reconstruction process are in Methods.

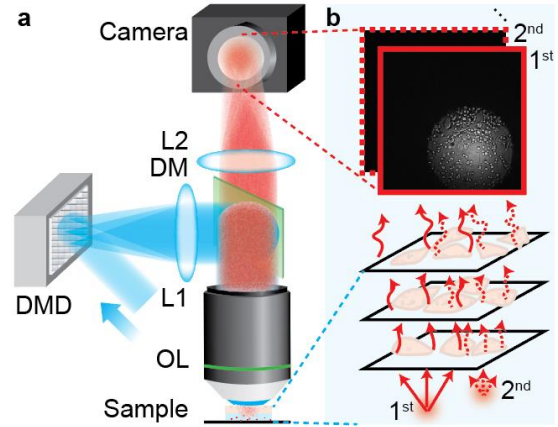


Fig. 1: Optical schematic diagram of Computational Hybrid Imaging (CHI). (a) A collimated beam is modulated by a digital micromirror device (DMD) to selectively excite fluorophores in the sample. Emitted fluorescence is scattered by the tissue above and collected by a camera. (b) Forward measurements of the multi-slice model with a zoom-in view of the sample. The sample consists of fluorescence-labeled structures on the bottom and non-fluorescence labeled tissue on the top. Fluorescence structures is modeled as incoherent spherical wave light sources. The non-fluorescence labeled tissue is modeled as a series of thin slices. Fluorescence propagating through the multiple slices carries both fluorescence signal and refractive index (RI) of the tissue. Various regions of the fluorescence structures are excited one-by-one in sequence and corresponding forward measurements are collected.

We first demonstrate CHI is able to reconstruct 3D RI from fluorescence images. The sample consists of two layers: the bottom layer of PDMS (RI 1.43) is about 150 μm thick with 0.71 μm red fluorescence beads inside as the light sources; the top layer of PDMS is about 100 μm thick with glass beads (RI 1.50, size 5-50 μm) inside as non-fluorescence objects (Fig. 2a). We illuminate the sample by scanning an $8 \times 8 \mu\text{m}^2$ spot across the whole field-of-view (FOV) to rapidly record raw forward measurements. All forward measurements are taken at the same axial plane. We then selected 21 images from the raw data as selected forward measurements. A representative forward measurement is shown in Fig. 2b, where we can tell a defocused fluorescence light source and glass beads. With the multi-slice model, the reconstructed RI clearly distinguishes single glass beads in a cluster, indicating a good optical sectioning ability (Fig. 2c-f). Fig. 2c and Fig. 2d are reconstructed result at two different axial planes that are 24 μm apart. To verify the reconstruction result, we took widefield images of the sample at several axial positions to identify the position of the glass beads (Fig. 2g-j). This image stack is taken under transmission illumination by an infrared LED and a motorized stage controls the axial position of the objective lens. Note the widefield images are not used for RI reconstruction. Therefore, this experimental result demonstrates the multi-slice model is able to reconstruct 3D RI from fluorescence images.

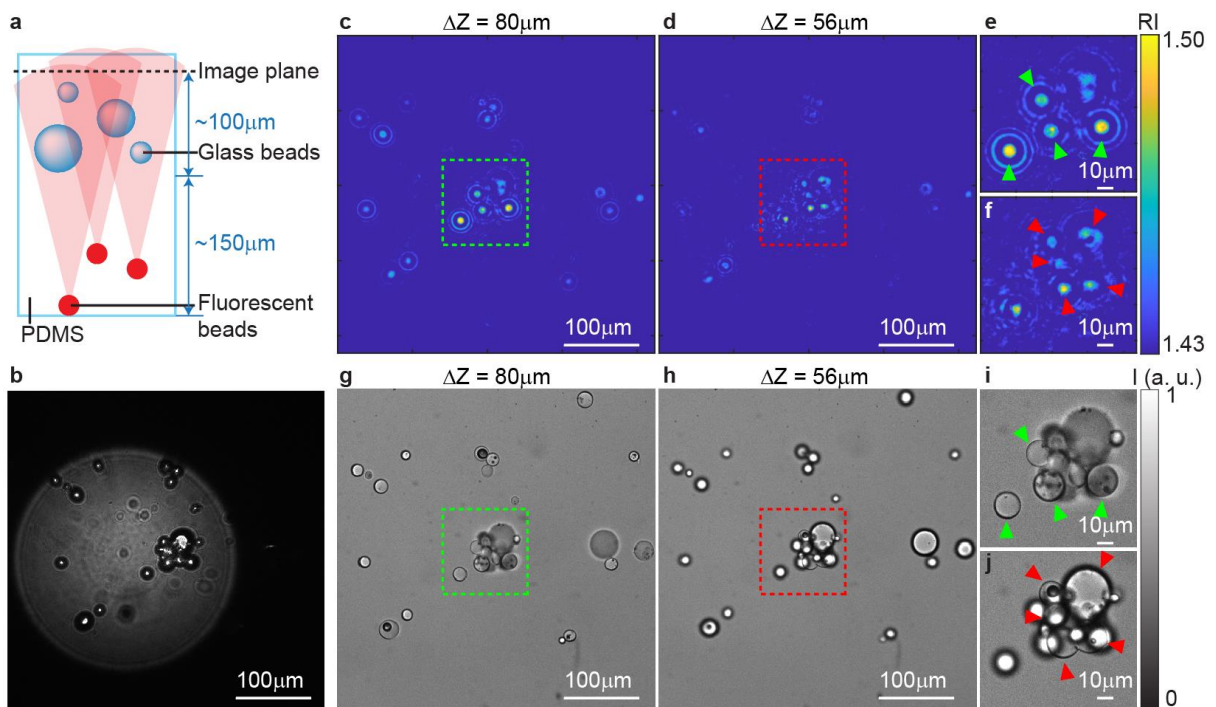


Fig. 2: CHI reconstructs 3D RI from experimentally measured fluorescence images. (a) The diagram of the sample. Fluorescent beads on the bottom layer of the PDMS play a role of 'light sources' and glass beads on the top layer of the PDMS act as non-fluorescence structures to be reconstructed. (b) A representative forward measurement. The image shows defocused fluorescence signal is scrambled by the glass beads. Totally 21 forward measurements are used in the reconstruction. (c, d) Reconstructed RI of glass beads at $\Delta z = 80 \mu\text{m}$ and $\Delta z = 56 \mu\text{m}$ below the image plane, respectively. (e, f) Zoom-in view of the dash box regions in (c) and (d). (g, h) Widefield images of the sample under transmitted illumination to show the position of the glass beads as a 'ground truth' to compare with the reconstruction results. (i, j) Zoom-in view of the dash box regions in (g) and (h). The color bar of RI is for (c-f) and the color bar of normalized intensity is for (b, g-j).

Next, we demonstrate CHI is able to reconstruct both 3D fluorescence and 3D RI from the same raw measurements. The sample is made by two steps: first, we fixed red fluorescent beads in PDMS on top of a coverslip; next, we coated the top surface of the PDMS with poly-lysine and cultured non-labeled CHO cells on it. During the experiment, we place the sample in phosphate-buffered saline solution (RI 1.33). Like the experiment above, we excite fluorescent beads in the sample with an $8 \times 8 \mu\text{m}^2$ spot scanning across the FOV and collect raw forward measurements (37×60 scanning steps, 2220 images). We select 23 fluorescence images as forward measurements for the multi-slice model. An example of the fluorescence image is shown in Fig. 3b. We treat the previous experiment of glass beads as a calibration reference and we used the same parameters in the optimization algorithm for reconstruction. The reconstructed 3D RI at $\Delta z = 40 \mu\text{m}$ below the image plane is shown in Fig. 3c, and Fig. 3d shows the corresponding widefield image under transmitted illumination as a ground truth of the cell position. This result shows the multi-slice model is able to reconstruct the 3D RI of alive cells.

Besides 3D RI of non-labeled objects, our method also can reconstruct 3D fluorescence objects in the sample from the same raw data. In addition to the 23 forward measurements used for RI reconstruction, we select another 125 forward measurements from the raw data to reconstruct 3D fluorescence. These 125 forward measurements either have low SNR or small light-up areas,

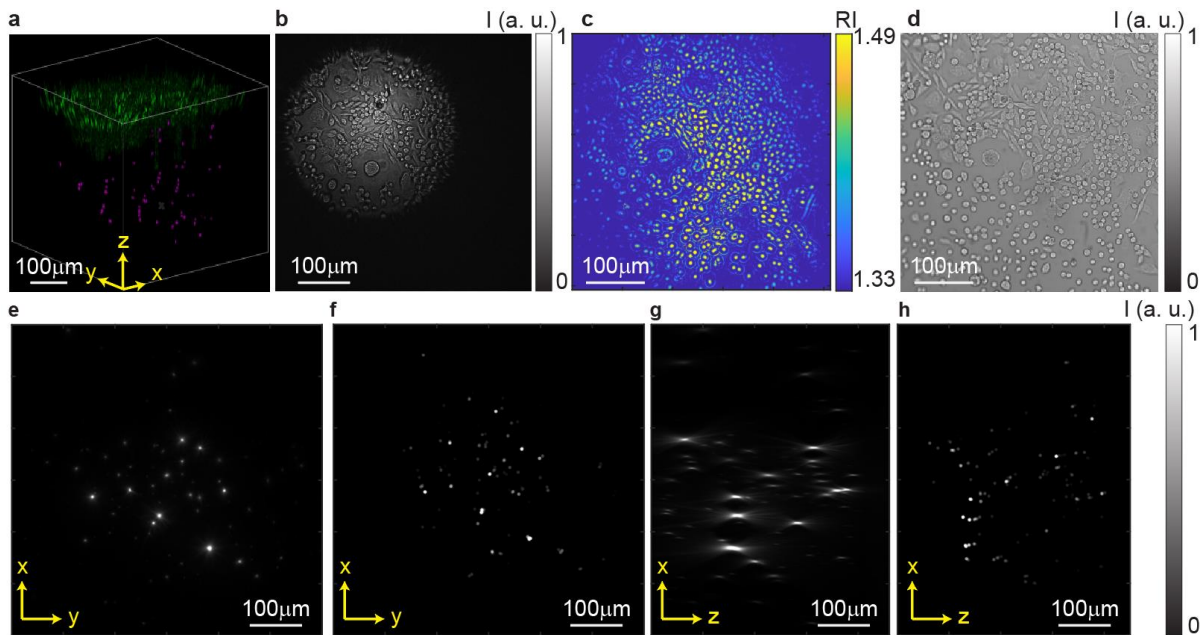


Fig. 3: CHI reconstructs both 3D fluorescence and 3D RI from a single dataset. (a) 3D registration of fluorescent signals from fluorescent beads (magenta) and RI from alive CHO cells (green) of the sample. (b) A representative image of the forward measurements. (c) Reconstructed 3D RI of CHO cells at $\Delta z = 40 \mu\text{m}$ below the image plane from 23 forward measurements. (d) Widefield image of the sample under transmitted infrared illumination to show the ground truth of the cells' position. (e, g) Maximum intensity projection (MIP) of widefield image stack under 473nm laser illumination in the reflective mode to show the ground truth of the fluorescent beads' location ((e) MIP in z-axis, (g) MIP in y-axis). Note this 3D fluorescence image stack is not used in the reconstruction of fluorescence distribution. (f, h) Reconstructed 3D distribution of the fluorescence beads' location ((f) MIP in z-axis, (h) MIP in y-axis) from 148 forward measurements like (b). (e-h) share the same color bar for normalized intensity.

which are not good forward measurements for RI reconstruction but still carry fluorescence information from dim or nearby fluorescence objects. Note that the selection of different forward measurements is off-line and tailored for the object without the requirement of additional experiments. The reconstruction results (Fig. 3f, 3h) indicate the location of fluorescent light sources. The intensity of the reconstructed scatter marker is proportional to the total intensity of the corresponding forward measurement. We also take a 3D axial-scanned image stack as the ground truth of fluorescence distribution under widefield illumination of 473nm laser (Fig. 3e, 3g). This image stack is not used in the reconstruction of Fig. 3f and Fig. 3h. Compared to the ground truth, our method can reconstruct most of fluorescence objects accurately at high spatial precision. Since the RI and fluorescence are reconstructed from the same raw forward measurements, we can easily and accurately register them back to the original locations in the 3D volume (Fig. 3a), which enables quantification of the spatial relationship between the fluorescence structures and non-labeled structures of the same sample.

Known the 3D RI not only provides a panoramic view of the sample beyond conventional fluorescence imaging, but also can digitally correct multiple scattering effect of fluorescence imaging. To demonstrate this application, we use a negative fluorescent USAF target as the fluorescence object, and an opaque glass-bead sample as the scattering phantom, with immersion oil (RI=1.515) in between (Fig. 4a). We first focus on the USAF target through the scattering glass-bead sample and take a widefield fluorescence image in focus (Fig. 4c-d). Then we move the focal plane above the glass-bead sample, like in the previous experiments, and collect the forward measurements by point-scanning the sample. We reconstruct the 3D RI of the glass-bead sample from 10 forward measurements. One representative plane of the reconstructed 3D RI is shown in Fig. 4b. Next, we calculate the scattered point-spread-function (PSF) with the reconstructed 3D RI. We perform Richardson-Lucy deconvolution to the scattered USAF image

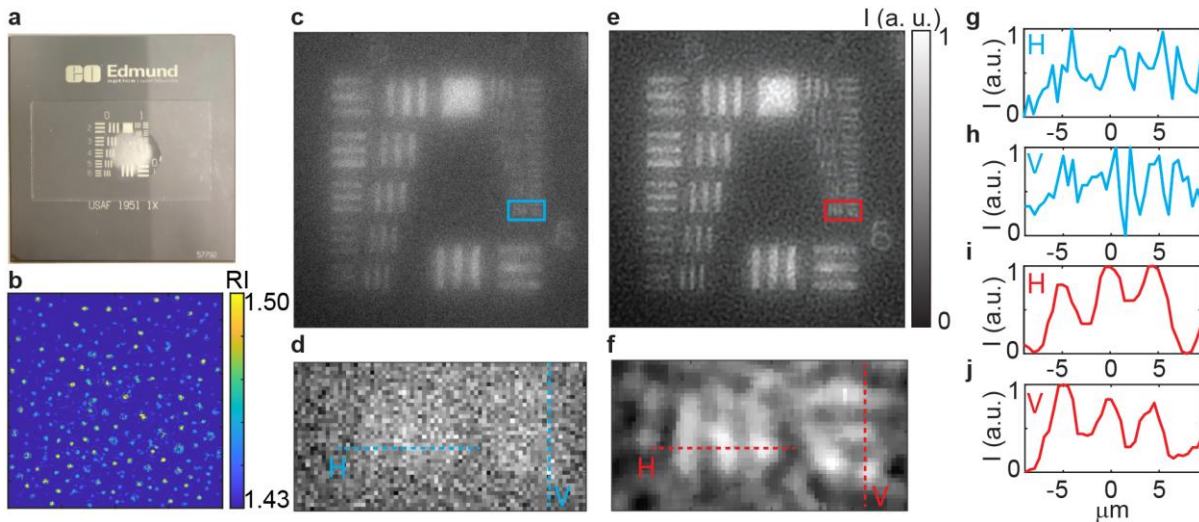


Fig. 4. CHI applies the reconstructed RI to digitally correct multiple scattering of fluorescence images. (a) A negative fluorescence USAF target is used as the fluorescence sample and an opaque glass-beads phantom on the top acts as the scattering media. (b) Reconstructed 3D RI. Only one 2D plane is shown here. (c) Raw fluorescence image of the USAF target under wide-field blue laser illumination. Different from forward measurements, this image is in focus. (d) Line pairs of Element 6 of Group 7. Zoom in view of the area in blue box in (c). (e) Reconstructed image after correcting multiple scattering with the multi-slice model. (f) Zoom in view of the area in red box in (e). (g-j). Normalized intensity profiles along the dash lines of corresponding color in (d) and (f).

(Fig. 4c-d) with the scattered PSF to correct the multiple scattering effect. The reconstructed image can clearly distinguish the finest line pairs (Element 6 of Group 7, 228.1 line pairs/mm) on the USAF target (Fig. 4e-f), whereas the scattered image cannot. Fig. 4g-j quantitatively compare the normalized intensity profiles of the line pairs in the scattered image (Fig. 4d) and in the reconstructed image (Fig. 4f) in both horizontal (H) and vertical (V) directions. The result shows one application of CHI that the reconstructed RI can be used to digitally correct multiple scattering effect and improve image SNR of fluorescence imaging.

In conclusion, CHI is a new imaging method that reconstructs 3D fluorescence and 3D RI from only fluorescence images by solving the inverse problem of multiple scattering based on a multi-slice model. We experimentally demonstrate the 3D reconstructed RI of glass beads and alive CHO cells registered with fluorescence beads in the same sample. We also demonstrate an application of CHI with the reconstructed RI by digitally correcting multiple scattering effect and improve the SNR of fluorescence images that are taken through a visually opaque phantom. CHI is in a reflective mode of microscopy and is compatible with both one-photon and multiphoton microscopy, which will facilitate a wide range of applications in biology. CHI demonstrates a proof-of-concept experiment to reconstruct RI information from fluorescence images, which is beyond the conventional applications of fluorescence microscopy.

Methods

Data availability. The datasets generated during and/or analyzed during the current study are available upon reasonable request to the corresponding authors.

Code availability. The codes generated during and/or analyzed during the current study are available upon reasonable request to the corresponding authors.

Computational reconstruction framework

1. Forward model

The forward measurements are taken by scanning a small spot across the FOV, which is denoted by $s(\mathbf{r} - \mathbf{r}_l)$ for l th illumination spot. We utilize sparsity-constrained inverse methods to recover the voxelized sparse 3D distributions of the fluorophores $o_f(\mathbf{r})$ from 2D camera measurements at a single axial plane $I(\mathbf{r}; z)$. This process can be modeled as

$$\hat{I}_l(\mathbf{r}; z) = [o_f(\mathbf{r}) \cdot s(\mathbf{r} - \mathbf{r}_l)] \otimes h_f(\mathbf{r}; z), \quad (2)$$

where $h_f(\mathbf{r}; z)$ is the intensity of PSF from each voxel at the image plane.

In terms of the RI reconstruction, the fluorescence light emitted from a fluorophore is denoted by a spherical wave $E_{0,l}(\mathbf{r}) = \frac{\exp(i\frac{2\pi}{\lambda}n_b\mathbf{r})}{r}$ which is the initial electric field of the multi-slice model at l th measurement, where \mathbf{r} donates the 3D spatial position vector, λ is the center wavelength of the fluorophore and n_b denotes the homogenous RI of the surrounding media. As the input electric field $E_{k,l}(\mathbf{r})$ passes through the k th ($k = 1, 2, \dots, N$) slice of the multi-slice model, the input electric field will be pointwise multiplied by the corresponding 2D transmittance function $t_k(\mathbf{r}) = \exp(i\frac{2\pi}{\lambda}\Delta z(n_k(\mathbf{r}) - n_b))$ at the corresponding z depth, where Δz denotes the propagation distance between slices and $n_k(\mathbf{r})$ denotes the complex-valued RI at k th layer. The output electric field is propagated in free space to the next slice by multiplying the mathematical operator

$\mathcal{P}\{\cdot\}$. According to the angular spectrum propagation method, $\mathcal{P}\{\cdot\} = \mathcal{F}^{-1}\{\exp(-i\Delta z\sqrt{(\frac{2\pi}{\lambda})^2 - \|\mathbf{k}\|^2})\mathcal{F}\{\cdot\}\}$, where $\mathcal{F}\{\cdot\}$ and $\mathcal{F}^{-1}\{\cdot\}$ denote 2D Fourier and inverse Fourier transforms, respectively, and \mathbf{k} denotes the spatial frequency vector. This process can be recursively written as

$$E_{k,l}(\mathbf{r}) = \mathcal{P}\{t_k(\mathbf{r}) \cdot E_{k-1,l}(\mathbf{r})\}.$$

The final forward measurement is the intensity of the exit electric field $E_N(\mathbf{r})$ on the top of the multi-slice volume, which is

$$\hat{I}_l(\mathbf{r}; z) = \left| \mathcal{F}^{-1}\{p(\mathbf{k}; z) \cdot \mathcal{F}\{E_{N,l}(\mathbf{r})\}\} \right|^2, \quad (4)$$

where $p(\mathbf{k}; z)$ is the pupil function corresponding to the image plane at z .

2. Reconstruction algorithm

Because both the position of fluorescence ‘light sources’ and the 3D RI are unknown, we need to reconstruct them jointly. Defining $e(o_f, n_k)$ as a joint-variable cost function that measures the difference between the raw intensity acquisitions $\{I_l(\mathbf{r}; z) | l = 1, 2, \dots, M\}$ and the expected intensities from estimated variables via the forward model. We estimate the fluorescence signals by solving the inverse problems with LASSO regularizer:

$$e_f(o_f) = \operatorname{argmin}_{o_f(\mathbf{r})} \sum_l \left\| I_l(\mathbf{r}; z) - [o_f(\mathbf{r}) \cdot s(\mathbf{r} - \mathbf{r}_l)] \otimes h_f(\mathbf{r}; z) \right\|_2^2 + \tau_f \|o_f(\mathbf{r})\|_1, \quad (5)$$

and we estimate the RI by solving the inverse problems with Tikhonov regularizer:

$$e_{RI}(n) = \operatorname{argmin}_{n(\mathbf{r})} \sum_l \left\| I_l(\mathbf{r}; z) - \hat{I}_l(\mathbf{r}; z) \right\|_2^2 + \tau_{RI} \|n(\mathbf{r})\|_2^2. \quad (6)$$

We solve both optimization problems with fast iterative shrinkage-thresholding algorithm (FISTA), which is a first-order gradient descent algorithm.

Optical setup

The laser source to excite fluorescence objects is a Diode Pumped Solid State (DPSS) laser diode at 473nm wavelength (MBL-N-473A-1W, Ultralasers, Inc., Canada). Current supplies are externally driven by an analog modulation voltage. The laser beam size is expanded to fill the DMD (DLP9000X and the controller V4390, ViALUX, Germany). The DMD is mounted on a rotation base to maximize the output laser power from ‘ON’ pixels and minimize the diffraction pattern from DMD pitches. Then the patterned beam passes through a tube lens ($f=180\text{mm}$) and the objective lens (XLUMPlanFL N, 20x, NA 1.0, Olympus) to generate illumination spot. The objective lens is mounted on a motorized z-stage (FG-BOBZ-M, Sutter Instrument, U.S.). A customized dichroic mirror (zt473/589/635rpc-UF2, Chroma, U.S.) is placed before the objective lens to reflect the stimulation laser beams while transmitting fluorescence photons emitted from the sample. Fluorescence images are recorded by a camera (Prime95B, Teledyne Photometrix, U.S.) with Micro-Manager software. The samples are placed on a motorized x-y stage (X040528 and the controller MP-285, Sutter Instrument, U.S.). A NI-DAQ (National Instruments, NI PCIe-6363) synthesizes custom analog signals to synchronously modulate the lasers, the DMD, and the camera. A custom MATLAB (MathWorks, U.S.) graphic user interface is used to control the

NI DAQ boards, calibrate and align the imaging modalities, and for data acquisition. Custom Python codes are used for data processing and reconstruction.

Sample preparation

The first step is to make fluorescence samples for experiments in Fig. 2-3. Red fluorescence beads suspension (R700, Thermo Fisher Scientific, MA) is mixed with PDMS (Sylgard 184, Dow Inc, MI) in the ratio of 1:550. Base elastomer and curing agent of PDMS are mixed in the ratio of 10:1. After mixing, we use a vacuum desiccator to remove the air bubbles in the mixture for 30min. Then the mixture is poured onto clean coverslips and heated at 100 Celsius for 35min. A fluorescence sample is finished. For the experiment in Fig. 2, we mix glass beads (SLGMS-2.5, Cospheric LLC, CA) with PDMS and then remove air bubbles with a vacuum desiccator. The mixture is poured onto the fluorescence sample and heated for curing. For the experiment in Fig. 3, we place Chinese hamster ovary (CHO) cells on the fluorescence samples coated with poly-D-lysine (Sigma-Aldrich, MO) one day before the experiment. CHO cells were maintained in Han's F-12 medium with L-glutamine (Thermo Fisher Scientific, MA) before the experiment and placed in phosphate-buffered saline (PBS, Thermo Fisher Scientific, MA) during the experiment. The glass-bead sample in Fig. 4 is made by mixing glass beads with PDMS in the ratio of 1:10 and then degasifying the mixture and curing it as described above. The glass-bead sample is placed onto a negative fluorescence USAF target (Edmund Optics, CA) with immersion oil (Resolve, Thermo Fisher Scientific, MA) in between.

Acknowledgements

This work was supported by DARPA N66001-17-C-40154 to Hillel Adesnik (H.A.) and L.W., as well as NIH UF1NS107574 to H.A. and L.W. This work was funded by the Gordon and Betty Moore Foundation's Data-Driven Discovery Initiative through Grant GBMF4562 to L.W. We thank Mr. David Ren in L.W. group to help debugging and Dr. Savitha Sridharan in H.A. group to help culturing cells.

References

1. Vellekoop, I. M. & Mosk, A. P. Focusing coherent light through opaque strongly scattering media. *Opt. Lett.* **32**, 2309–2311 (2007)
2. Mosk, A. P., Lagendijk, A., Leroose, G. & Fink, M. Controlling waves in space and time for imaging and focusing in complex media. *Nat. Photonics* **6**, 283 (2012)
3. Gigan, S. Optical microscopy aims deep. *Nat. Photonics* **11**, 14–16 (2017)
4. Kobayashi, M., Mizumoto, T., Shibuya, Y., Enomoto, M. & Takeda, M. Fluorescence tomography in turbid media based on acousto-optic modulation imaging. *Appl. Phys. Lett.* **89**, 181102 (2006)
5. Si, K., Fiolka, R. & Cui, M. Fluorescence imaging beyond the ballistic regime by ultrasound pulse guided digital phase conjugation. *Nat. Photonics* **6**, 657–661 (2012)
6. Wang, Y. M., Judkewitz, B., DiMarzio, C. A. & Yang, C. Deep-tissue focal fluorescence imaging with digitally time-reversed ultrasound-encoded light. *Nature Communications* vol. 3 (2012)
7. Ruan, H., Liu, Y., Xu, J., Huang, Y. & Yang, C. Fluorescence imaging through dynamic scattering media with speckle-encoded ultrasound-modulated light correlation. *Nat. Photonics* **14**, 511–516 (2020)

8. Popoff, S., Lerosey, G., Fink, M., Boccarda, A. C. & Gigan, S. Image transmission through an opaque material. *Nat. Commun.* **1**, 81 (2010)
9. Popoff, S. M. et al. Measuring the transmission matrix in optics: an approach to the study and control of light propagation in disordered media. *Phys. Rev. Lett.* **104**, 100601 (2010)
10. Kang, S. et al. Imaging deep within a scattering medium using collective accumulation of single-scattered waves. *Nat. Photonics* **9**, 253 (2015)
11. Yoon, S. et al. Deep optical imaging within complex scattering media. *Nature Reviews Physics* **2**, 141–158 (2020)
12. Moretti, C. & Gigan, S. Readout of fluorescence functional signals through highly scattering tissue. *Nat. Photonics* **1–4** (2020)
13. Xue, Y. et al. Scattering reduction by structured light illumination in line-scanning temporal focusing microscopy. *Biomed. Opt. Express*, *BOE* **9**, 5654–5666 (2018)
14. Wadduwage, D. N., Park, J. K., Boivin, J. R., Xue, Y. & So, P. T. C. De-scattering with Excitation Patterning (DEEP) Enables Rapid Wide-field Imaging Through Scattering Media. *arXiv [physics.optics]* (2019)
15. Wei, Z. et al. 3D Deep Learning Enables Fast Imaging of Spines through Scattering Media by Temporal Focusing Microscopy. *arXiv [eess.IV]* (2019)
16. Escobet-Montalbán, A. et al. Wide-field multiphoton imaging through scattering media without correction. *Sci Adv* **4**, eaau1338 (2018)
17. Choi, W. et al. Tomographic phase microscopy. *Nat. Methods* **4**, 717–719 (2007)
18. Sung, Y. et al. Optical diffraction tomography for high resolution live cell imaging. *Opt. Express* **17**, 266–277 (2009)
19. Kim, T. et al. White-light diffraction tomography of unlabelled live cells. *Nature Photonics* vol. 8 256–263 (2014)
20. Tian, L. & Waller, L. 3D intensity and phase imaging from light field measurements in an LED array microscope. *Optica*, *OPTICA* **2**, 104–111 (2015)
21. Chowdhury, S. et al. High-resolution 3D refractive index microscopy of multiple-scattering samples from intensity images. *Optica*, *OPTICA* **6**, 1211–1219 (2019)
22. Li, J. et al. High-speed *in vitro* intensity diffraction tomography. *AP* **1**, 066004 (2019)
23. Chen, M., Ren, D., Liu, H.-Y., Chowdhury, S. & Waller, L. Multi-layer Born multiple-scattering model for 3D phase microscopy. *Optica*, *OPTICA* **7**, 394–403 (2020)
24. Liu, H.-Y. et al. 3D imaging in volumetric scattering media using phase-space measurements. *Opt. Express* **23**, 14461–14471 (2015)
25. Zhou, K. C., Qian, R., Degan, S., Farsiu, S. & Izatt, J. A. Optical coherence refraction tomography. *Nat. Photonics* **13**, 794–802 (2019)
26. Kim, K. et al. Correlative three-dimensional fluorescence and refractive index tomography: bridging the gap between molecular specificity and quantitative bioimaging. *Biomed. Opt. Express* **8**, 5688–5697 (2017)
27. Shin, S., Kim, D., Kim, K. & Park, Y. Super-resolution three-dimensional fluorescence and optical diffraction tomography of live cells using structured illumination generated by a digital micromirror device. *Sci. Rep.* **8**, 9183 (2018)
28. Chung, J., Kim, J., Ou, X., Horstmeyer, R. & Yang, C. Wide field-of-view fluorescence image deconvolution with aberration-estimation from Fourier ptychography. *Biomed. Opt. Express* **7**, 352–368 (2016)
29. Yeh, L.-H., Chowdhury, S. & Waller, L. Computational structured illumination for high-content fluorescence and phase microscopy. *Biomed. Opt. Express* **10**, 1978–1998 (2019)